arXiv:1403.7716v1 [cond-mat.mes-hall] 30 Mar 2014

Extracting entangled qubits from Majorana fermions through the measurement of parity

Li Dai (戴笠),[1] Watson Kuo (郭華丞),[1,2] and Ming-Chiang Chung (張明強)[1,3,*]

[1] *Department of Physics, National Chung Hsing University, Taichung, 40227, Taiwan*
[2] *Center of Nanoscience and Nanotechnology, and Institute of Nanoscience, National Chung Hsing University, Taichung 40227, Taiwan*
[3] *Physics Division, National Center for Theoretical Science, Hsinchu, 30013, Taiwan*

(Dated: April 1, 2014)

We propose a scheme for extracting entangled charge qubits from quantum-dot chains that support zero-energy edge modes. The edge mode is composed of Majorana fermions localized at the ends of each chain. The qubit, logically encoded in double quantum dots, can be manipulated through tunneling and pairing interactions between them. The detailed form of the entangled state depends on both the parity measurement (an even or odd number) of the inner-site electrons in each chain and the teleportation between the chains. The parity measurement is realized through employing coherent-state microwave photons to interact with the inner sites, while the teleportation is performed in a way similar to qubit manipulations. Our scheme provides an illustration of *localizable entanglement*, which is feasible under realistic experimental conditions, as it allows for finite temperature effect as well as disorders and decoherence of the system.

I. INTRODUCTION

Majorana fermions (MFs), first considered by Ettore Majorana in 1937 for decomposing Dirac fermions into a superposition of real fermions [1], are hypothetical particles which are their own antiparticles. In particle physics, no elementary particles are MFs except the neutrino whose nature is not explicitly resolved [2]. In condensed matter physics, however, MFs have been proposed as quasi-particle excitations of the $\nu = 5/2$ fractional quantum Hall state [3], at the surface of a topological insulator coupled with a s-wave superconductor [4], in the quantum wells or quantum wires [5–7], and in cold atoms [8]. Generally, three elements are needed for the realization of MFs [9, 10]: strong spin-orbit interaction to generate position or momentum dependent spin directions, superconductivity to induce electrons pairing effect, and Zeeman magnetic field to lift the spin degeneracy. Several experiments have been performed which can be interpreted as emergence of MFs [11–13].

MFs are interesting not only due to their fundamental properties but also in the aspect of their potential applications such as topological quantum computation [14], quantum state transfer [15], quantum memory [16] and fault-tolerant quantum random-number generation [17]. The unique feature of these applications is the topological phase of matter for which the manipulations in the degenerate ground state subspace are protected from local noise and thermal excitations are suppressed by a sizable energy gap [18].

In this work we propose a scheme for extracting entangled qubits from Majorana fermions through the measurement of parity. The system we consider is two parallel chains of quantum dots as shown in Fig. 1. Each chain is divided into two subchains. We will demonstrate that, under realistic experimental conditions, each subchain encompasses a zero-energy edge mode composed of two unpaired Majorana fermions. The edge mode corresponds to two degenerate ground states for which the inner sites of the sub-chain (the bulk) are generally entangled with the boundary sites (the edges). The states for the bulk part in this bulk-edge entangled state have a definite parity (an even or odd number of electrons), while for the edges they are themselves (maximally) entangled states between the boundary sites. We propose employing coherent microwave photons to interact with the bulk in order to measure its parity. In this way, the

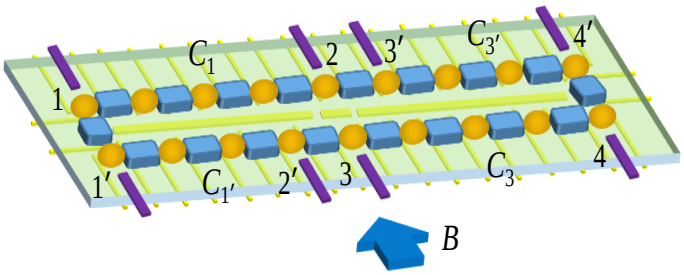

FIG. 1. (color online). The schematic diagram of the experimental setup for extracting entangled qubits from two parallel chains that support Majorana fermions. The quantum dots (dark yellow ellipsoids) and the superconducting grains (blue cuboids) are grown on a dielectric slab (silicon nitride). In the back of the slab, there is a grid of electrical gates (golden bars) for controlling the confining potential of the quantum dots as well as the couplings between the quantum dots and the superconducting grains. Each of the two parallel chains are labeled as two connected chains. The chemical potential of their boundary sites are controlled by the front gates (purple). A magnetic field $\boldsymbol{B}$ is applied perpendicularly to the chains to induce spin-split levels in the quantum dots.

* mingchiangha@phys.nchu.edu.tw

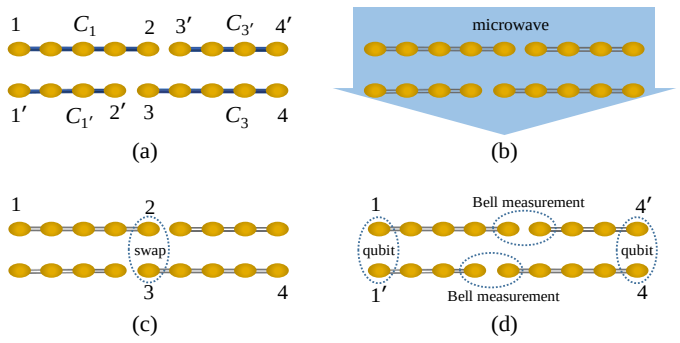

FIG. 2. (color online). The flow diagram $(a) \rightarrow (d)$ for extracting entangled qubits from two parallel chains that support zero-energy edge modes. (a) The two parallel chains, divided into four sub-chains, are initialized in the respective ground states. Each ground state is a bulk-edge entangled state. (b) A micorowave is incident on the chain to measure the parity of the bulk of each sub-chain, in order to collapse the wave function into an entangle state of the boundary sites (See Fig. 4(b) for details). Here the hollow grey lines indicate that the interactions between neighboring sites in the sub-chains are swtiched off. (c) A swap operation between the site 2 and 3 is performed, resulting in a bipartitie entangled state where the two subsystems are $(1, 3)$ and $(2, 4)$. The sequence of (c) and (d) can be interchanged. (d) Two Bell measurements are perfromed in order to teleport the state of 3 to $1'$ and that of 2 to $4'$. In this way, entangle qubits are formed in the overall ends of the two parallel chains. The step (b) can be postponed after (c) and/or (d).

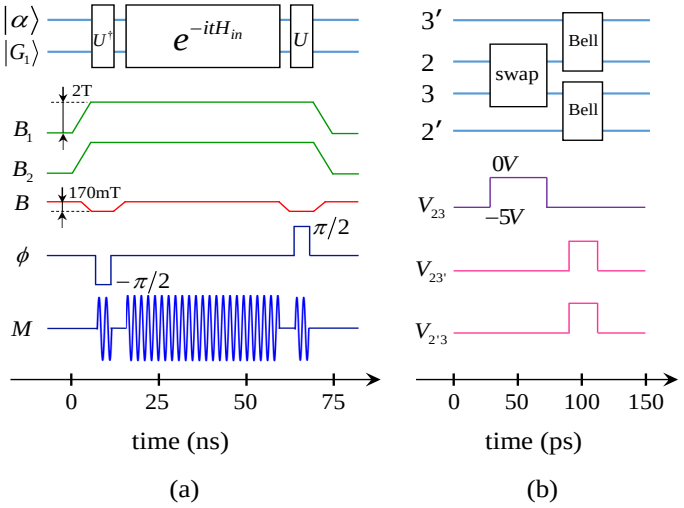

FIG. 3. (color online). The schematic diagram of the principal pulse sequence of our scheme for illustrative purposes only. (a) shows the process of measuring the parity of the inner-site electrons of one sub-chain. It corresponds to Fig. 2 (b). Here the microwave initally in the coherent state $|\alpha\rangle$ and the sub-chain C_1 will go through three interactions $U^\dagger, e^{-itH_{in}}, U$ designated by Eq. (10). B_1, B_2 are local nanoscale magentic fields applied to the site 1 and 2 resepctively. They are used to adiabatically increase the spin-split gap by a considerable amount so as to effectively switch off the interaction of the two sites with the microwave. B is the original Zeeman field. Decreasing it by 28.75 mT is to tune the gap of inner-site electrons into resonance with the microwave for realizing $U^\dagger, U$. ϕ and M are the phase and waveform of the microwave. (b) corresponds to Fig. 2 (c) and (d). Here V_{jk} is the gate voltage between the site j and k. Increasing it will decrease the potential barrier, which induces an intraction between the relevant sites.

maximally entangled edge states can be extracted. It can be seen that our proposal illustrates the concept of *localizable entanglement* [19, 20]. However, the edge states are not good entangled qubits, because the basis for the states is encoded in a single fermionic site, so that a superposition between the basis states is difficult [21, 22]. We propose a scheme to transform the edge states into two useful entangled qubits encoded in the boundary sites of the parallel chains so that superposition states of the qubit are allowed. The scheme involves a swap operation between the sites of different edge states, and teleportation through the edge states. Fig. 2 and 3 show the flow diagram and principal pulse sequence of our scheme. The total operation time ~ 75 ns$\times 4 + 150$ ps ≈ 300 ns (see Fig. 3) is within the decoherence time ~ 700 ns mainly due to the Johnson-Nyquist noise of the electric gates [23]. Another common source of decoherence is the environmental charges trapped in the insulating substrate or at the interface of the heterostructure [24]. These random charges interact with the electrons in the quantum dot, which causes severe decoherence. New growth methods for materials with low trapped charge density [25], as well as the charge echo techniques [26], can alleviate the decoherence.

The entangled qubits extracted are a useful entanglement resource in the teleportation-based quantum computation (TQC) which is equivalent to the one-way quantum computation [27, 28]. TQC can be used as a supplement to the standard charged-based quantum computing (CQC) [23] in the situations where quantum gates between remote qubits are needed, with the other ingredients: two- and three-qubit measurements realized by CQC. Our proposal allows for finite temperature effect, as the ground state of the chain is protected by a substantial energy gap induced by the superconducting proximity effect. Also, it is only required to finely tune the system parameters close to the edges, while small disorders of the system in the bulk of the chain is allowed. Therefore, our proposal can be implemented under realistic experimental conditions.

The rest of the paper is organized as follows. In Sec. II, we study the model for describing the system in Fig. 1 and discuss the range of the parameters that supports perfect localized edge modes. We also show that the edge mode corresponds to the boundary sites in maximally entangled states correlated (entangled) with the parity-distinct states of the inner sites. In Sec. III, we discuss a scheme for realizing the measurement of the parity. The scheme, employing coherent-state microwave photons to

interact with the inner sites, is crucial for obtaining entangled states of the boundary sites. In Sec. IV, we show that the obtained entangled states can be transformed, by using a swap operation and teleportation, into entangled qubits located at the overall ends of the two parallel chains. Finally, we give a conclusion in Sec. V.

II. THE MODEL

For convenience of discussion, each chain in Fig. 1 is re-labelled as two connected sub-chains so that there are four sub-chains $C_1, C_{1'}, C_3, C_{3'}$, with respective boundary sites being $(1,2),(1',2'),(3,4),(3',4')$. The partition scheme is not unique, as long as the sites 2 and 3 are aligned to allow a controllable coupling between them. The system of a single chain has already been proposed by Sau and Sarma for realizing MFs [29]. We briefly review the experimental realization of the chain. The linear chain with N sites is composed of N quantum dots. The two adjacent quantum dots are coupled through s-wave superconductors which induce pairing interaction in the quantum dots [30]. A Zeeman magnetic field $\boldsymbol{B}$ is perpendicularly applied to the chain, lifting the spin degeneracy, so that only a single quantum level effectively participates in the interaction between neighboring quantum dots. The chemical potential of each quantum dot is tuned by applying gate voltages individually, in order to resonantly couple the lower spin-split level of quantum dots to the Fermi level of superconductors. The gate voltages also induce Rashba spin-orbit interaction in the quantum dots, which results in spin texture in the quantum level indispensable for generating proximity effect in the neighboring sites [5, 6]. The chain is shown [29] to support a zero-energy Majorana edge mode for a wide range of system parameters with disorders. The edge mode is topologically protected against local perturbation and thermal noise is also suppressed due to the substantial energy gap of the chain [18].

We study one sub-chain first. This corresponds to switching off the couplings between any two of the four sub-chains through performing appropriate electrical gating operations. The effective Hamiltonian is [29, 31]

$$H=\sum_{j=1}^{N-1}(-w_j c_j^\dagger c_{j+1}+\Delta_j c_j c_{j+1}+h.c.)-\sum_{j=1}^{N}\mu_j c_j^\dagger c_j, \tag{1}$$

where the operator $c_j^\dagger$ (c_j) creates (annihilates) an electron in the Fermi level (the lower spin-split level with energy μ_j) of the jth quantum dot, w_j and Δ_j are the tunneling and pairing amplitudes between the jth and $(j+1)$th quantum dots. The subscripts here only describe the quantum dots in a sub-chain. Their meanings are different from the labelling for the boundary sites in Fig. 1. The parameters w_j, Δ_j and μ_j can be different from site to site, due to the limited precision in fabricating and controlling quantum dots. We assume $w_j>0$, as the phases of w_j can be eliminated by an appropriate transformation $c_k\to c_k e^{i\theta_k}$. Also, Δ_j is chosen to be a real number with a fixed sign (all positive or all negative) through carefully tuning the phases of the superconducting grains [29].

The Majorana operators are defined as follows

$$\begin{aligned} d_{2j-1}&=c_j+c_j^\dagger,\\ d_{2j}&=-i(c_j-c_j^\dagger), \qquad j=1,2,\cdots,N. \end{aligned} \tag{2}$$

Eq. (1) can be written in terms of d_{2j-1}, d_{2j},

$$\begin{aligned} H=&\frac{i}{2}\sum_{j=1}^{N-1}[(w_j+\Delta_j)d_{2j}d_{2j+1}+(-w_j+\Delta_j)d_{2j-1}d_{2j+2}]\\ &-\frac{i}{2}\sum_{j=1}^{N}\mu_j d_{2j-1}d_{2j}, \end{aligned} \tag{3}$$

We notice that when

$$\mu_1=\mu_N=0,\ \Delta_1=w_1,\ \Delta_{N-1}=w_{N-1}, \tag{4}$$

the Majorana operators d_1 and d_{2N} will be absent from Eq. (3). The two operators form a zero-energy edge mode with its annihilation operator

$$\tilde{b}_N=\frac{1}{2}(d_1+i\eta d_{2N})=\frac{1}{2}(c_1+c_1^\dagger+\eta c_N-\eta c_N^\dagger), \tag{5}$$

where $\eta=\det W_0$ with W_0 being a $(2N-2)\times(2N-2)$ real orthogonal matrix that block diagonalizes the coefficient matrix in Eq. (3) (its dimension is reduced by 2 due to the absence of d_1, d_{2N}), and $\eta^2=1$. The remaining Majorana operators $d_j, (2\le j\le 2N-1)$ form Dirac modes $\tilde{b}_k, (1\le k\le N-1)$ with generally non-zero energies. See Fig. 4(a). The introduction of η in Eq. (5) is to ensure that the parity operators of the respective Dirac modes are equal: $\prod_{j=1}^{N}(1-2c_j^\dagger c_j)=\prod_{j=1}^{N}(1-2\tilde{b}_j^\dagger\tilde{b}_j)$. Here the parity operator has two eigenvalues ±1. The eigenvalue 1 means the number of electrons (or quasi-particles for $\tilde{b}_j^\dagger\tilde{b}_j$) is even, while -1 means the corresponding number is odd. The Dirac modes $\tilde{b}_k$ diagonalize Eq. (3): $H=\sum_{k=1}^{N-1}\lambda_k(\tilde{b}_k^\dagger\tilde{b}_k-\frac{1}{2})$. See Appendix A for a detailed discussion.

The zero-energy mode $\tilde{b}_N^\dagger\tilde{b}_N$ corresponds to two-fold degenerate ground states with definite parity:

$$\begin{aligned} |G_1\rangle&=|\tilde{0}\rangle_1|\tilde{0}\rangle_2\cdots|\tilde{0}\rangle_{N-1}|\tilde{0}\rangle_N,\\ |G_2\rangle&=\tilde{b}_N^\dagger|G_1\rangle=|\tilde{0}\rangle_1|\tilde{0}\rangle_2\cdots|\tilde{0}\rangle_{N-1}|\tilde{1}\rangle_N. \end{aligned} \tag{6}$$

They satisfy $\tilde{b}_k|G_1\rangle=\tilde{b}_k|G_2\rangle=0, (k=1,2,\cdots,N-1)$, $\tilde{b}_N|G_1\rangle=0$, and $\tilde{b}_N^\dagger|G_2\rangle=0$. The actual ground state of the chain alternates between $|G_1\rangle$ and $|G_2\rangle$ through electron tunneling between the chain's boundary sites and the reservoir [32]. The tunneling is switched off through appropriately tuning the confining potentials, in order to fix the ground state. To determine the ground state, that

is, to measure its parity while keeping the state intact, the microwave scheme in Sec. III can be used. Alternatively, one can use Josephson junctions to measure the parity [33]. In fact, it's not necessary to know the state of the chain. One simply needs to ensure the state is the same ground state when it is repeatedly prepared. This can be done via precisely initializing the chain and controlling the time for approaching equilibrium. Then the state can be assumed to be $|G_1\rangle$. One checks the experimental results regarding entanglement (Sec. IV) and compares them with the theoretical calculations for $|G_1\rangle$. If the results are consistent, the initial assumption is correct. Otherwise, the initial state is $|G_2\rangle$.

In the solution (4), w_k, Δ_k for $2 \le k \le N-2$ and μ_k for $2 \le k \le N-1$ are arbitrary. However, their values will influence the energy gap ($\sim \text{Min}(2|\Delta_k|)$, $1 \le k \le N-1$ in the condition that $\Delta_j \approx w_j$ and $\mu_j \approx 0$ throughout the chain, see Ref. [29]).

By using $\tilde{b}_N|G_1\rangle = 0$ and $\tilde{b}_N^\dagger|G_2\rangle = 0$, it is not difficult to find out the forms of the two ground states in real space of the chain. (The details are presented in Appendix B.)

$$|G_1\rangle = x_0|\Phi^{(\eta)}\rangle_{1,N}|S_e\rangle + x_1|\Psi^{(\eta)}\rangle_{1,N}|S_o\rangle,$$
$$|G_2\rangle = x_0|\Psi^{(\eta)}\rangle_{1,N}|S_e\rangle + x_1|\Phi^{(\eta)}\rangle_{1,N}|S_o\rangle, \qquad (7)$$

where the states $|\Phi^{(\eta)}\rangle_{1,N} = (|00\rangle_{1,N} + \eta|11\rangle_{1,N})/\sqrt{2}$ and $|\Psi^{(\eta)}\rangle_{1,N} = (|10\rangle_{1,N} + \eta|01\rangle_{1,N})/\sqrt{2}$ are maximally entangled states between the boundary sites 1 and N, $|S_e\rangle$ and $|S_o\rangle$ are some states in general forms for the sites from 2 to $N-1$, and x_0, x_1 are coefficients to be determined. For $N = 2$, there are no inner sites and the two degenerate ground states are reduced to $|\Phi^{(\eta)}\rangle_{1,N}$ and $|\Psi^{(\eta)}\rangle_{1,N}$, which has been considered in Ref. [30]. Although x_0, x_1 are unknown, the expressions of the states (7) are sufficient for our discussion. The important aspect is the structure of these states: $|G_1\rangle, |G_2\rangle$, already written in the Schmidt decomposition form, are generally an entangled state between the boundary (edges) and the inner (bulk) sites of the chain. The Schmidt basis states of this bulk-edge entangled state have a definite parity (an even or an odd number of electrons) for the bulk: the parity of $|S_e\rangle$ ($|S_o\rangle$) is even (odd), while for the edges they are themselves (maximally) entangled states between the boundary sites. When the parity of the bulk is even, the two edges for $|G_1\rangle$ are in the state: $|\Phi^{(\eta)}\rangle_{1,N}$. When it is odd, they are in the state: $|\Psi^{(\eta)}\rangle_{1,N}$. The two states are both maximally entangled. The states $|\Phi^{(\eta)}\rangle_{1,N}$ and $|\Psi^{(\eta)}\rangle_{1,N}$ are interchanged for $|G_2\rangle$. We refer to Eq. (7) as conditionally maximally entangled states of the boundary sites. The four sub-chains in Fig. 1 will have four respective states of this type.

The parameter η is determined by w_j, Δ_j, μ_j in Eq. (3). When $\eta = 1$, the process of diagonalizing (3) corresponds to a *proper rotation* with the real orthogonal matrix W_0 acting on the vector $\vec{d} = (d_2, d_3, \cdots, d_{2N-1})$. The case of $\eta = -1$ is an *improper rotation* which includes a reflection operation on $\vec{d}$. It is numerically found that when

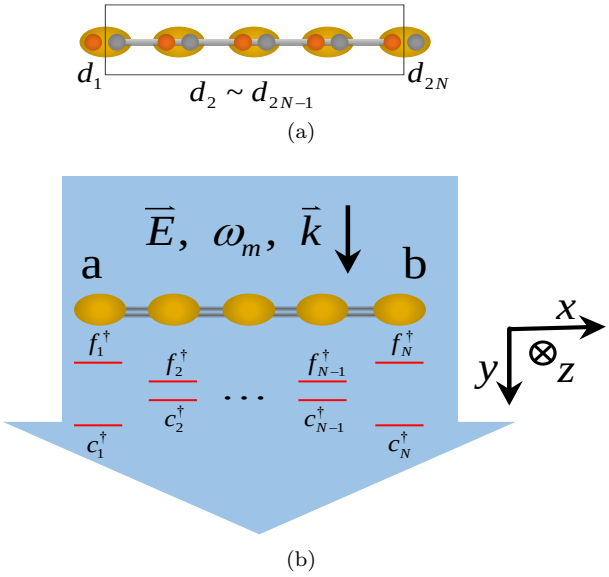

FIG. 4. (color online). (a) A quantum-dots chain with N fermionic sites ($N = 5$) is represented by $2N$ MFs (each site by two MFs). The two boundary MFs are unpaired for the parameter values in Eq. (4). They form a zero-energy mode, while all the other MFs are fused to form $N-1$ new fermions. (b) The diagram of employing microwave (its electric field $\vec{E}$, frequency ω_m and wave vector $\vec{k}$) to measure the parity of the inner-site electrons of a sub-chain, with $f_j^\dagger/c_j^\dagger$ the creation operator of the upper/lower spin-split energy level (red line) of the jth quantum dot.

$\Delta_j \approx w_j > 0$, $\mu_j \approx 0$, then $\eta = 1$. This is the parameter regime that we would like to consider, while the case $\eta = -1$ involves changing the signs of an odd number of w_j and Δ_j (a reflection operation) which is not a typical situation in experiments. Therefore, without loss of generality, we will assume $\eta = 1$.

III. EXPERIMENTAL SCHEME FOR REALIZING PARITY MEASUREMENT

The scheme for measuring the parity of the inner-site electrons of a sub-chain is shown in Fig. 4(b). First, we shall summarize the overall process. A microwave in a coherent state $|\alpha\rangle$ is incident on the chain along the y direction. The chain is in the ground state e.g. $|G_1\rangle$. After a proper time of interaction, the state becomes

$$x_0|\Phi^{(\eta)}\rangle_{1,N}|S_e\rangle|\alpha\rangle) + x_1|\Psi^{(\eta)}\rangle_{1,N}|S_o\rangle|-\alpha\rangle, \qquad (8)$$

where $|\pm\alpha\rangle$ are the coherent states of the microwave with the respective amplitude $\pm\alpha$. It can be seen that the state of the boundary sites will collapse to $|\Phi^{(\eta)}\rangle_{1,N}$ or $|\Psi^{(\eta)}\rangle_{1,N}$ through measuring the coherent states of the microwave, provided the coherent states are orthogonal. The orthogonality can be achieved to a good approximation when the amplitude α is sufficiently large so that

$|\langle\alpha|-\alpha\rangle|^2 = e^{-4|\alpha|^2} \ll 1$). The two coherent states can be measured by means of beam splitters and photodetectors, with the error rate of distinguishing the states smaller than 10^{-4} when $\alpha \geq 1.5$ [34].

The remaining part of the section will concentrate on the derivation of Eq. (8). First, we suddenly increase the strength of the confining potential in the x direction for each quantum dot of the sub-chain so that the tunneling and pairing interaction between neighboring sites are switched off. This is a process of quantum quench. The Hamiltonian is suddenly changed to the one with only the on-site terms in Eq. (1). We work in the interaction picture where the ground state will not evolve with time. Then, we adiabatically increase the gap between the spin-split levels of the two boundary quantum dots of the sub-chain so that it is much larger than the gap of the inner sites. This is performed through adiabatically increasing the nanoscale magnetic fields on the boundary site [35]. Subsequently, a microwave with frequency ω_m is incident on the chain along y-axis (see Fig. 4(b)), which is perpendicular to both the Zeeman field (along z-axis) and the chain. The microwave only effectively interacts with inner-site elctrons, since the resonant frequency of the boundary-site electron is far-detuned from the microwave frequency. The effective Hamiltonian with rotating-wave approximation is [36]

$$H_{in} = \delta \sum_{j=2}^{N-1} f_j^\dagger f_j + J \sum_{j=2}^{N-1} (e^{i\phi} a f_j^\dagger c_j + h.c.), \qquad (9)$$

where $\delta = \Omega - \omega_m$ is the detuning between the resonant frequency (Ω) of the quantum dots (the energy gap of the spin-split levels,) and the frequency (ω_m) of the microwave photons, $c_j, c_j^\dagger$ are defined in Eq. (1), $f_j(f_j^\dagger)$ is the annihilation (creation) operator for the upper spin-split level of the jth quantum dot around the Fermi level (see Fig. 4(b)), $a^\dagger, a$ are the creation and annihilation operators of the microwave photons, J is proportional to the coupling strength between the microwave and the quantum dots, and ϕ is the phase of the microwave. The Hamiltonian is written in the interaction picture with the free part $H_0 = \omega_m(a^\dagger a + \frac{1}{2} + \sum_{j=2}^{N-1} f_j^\dagger f_j)$. For realistic experiments where four chains are involved, the other three chains should also be adiabatically engineered in a similar way as that for the boundary sites of the chain under measurement. This is to effectively switch off the interaction of the microwave with these chains. Alternatively, one can use semiconductor photomasks to cover the boundary sites, and also the liquid crystal technology [37] to control the region for the microwave to pass through, only to the range of the chain under measurement. The phase ϕ in the above Hamiltonian can be adjusted by applying electric field via the electro-optic effect such as Kerr effect [38].

The Hamiltonian (9) is essentially the Tavis-Cummings (TC) model [39] for describing the interaction between photons and a set of two-level atoms, if we define the raising and lowering operators for the atom as $\sigma_j^\dagger = f_j^\dagger c_j$, $\sigma_j = c_j^\dagger f_j$. The anti-commutator $\sigma_j^\dagger\sigma_j + \sigma_j\sigma_j^\dagger = f_j^\dagger f_j + c_j^\dagger c_j - 2 f_j^\dagger f_j c_j^\dagger c_j = 1$ is fulfilled when there is exactly one electron in the two spin-split levels around the Fermi level. However, when there is no electron around the Fermi level of some site, the above anti-commutator equals 0 and thus is not well-defined. In this situation, the microwave will not effectively interact with that specific site. Therefore, the number of the two-level atoms (denoted as N_0) in the essential TC model is not fixed; it depends on the number of electrons around the Fermi levels of inner sites. The parity of this number is what we want to measure.

Next we apply a unitary transformation $U = \exp[\frac{J}{\delta}\sum_j (a\sigma_j^\dagger - a^\dagger\sigma_j)]$ to the Hamiltonian (9) for $\phi = 0$. Expanding to second order in J/δ, we have [40, 41]

$$H'_{in} = UH_{in}U^\dagger \approx (\delta + \tfrac{J^2}{\delta})\sum_j \sigma_j^\dagger\sigma_j + \tfrac{J^2}{\delta}\sum_j \sigma_j^z a^\dagger a + \tfrac{J^2}{\delta}(\sum_{j\neq k}\sigma_j^\dagger\sigma_k + \sigma_j\sigma_k^\dagger), \qquad (10)$$

where $\sigma_j^z = \sigma_j^\dagger\sigma_j - \sigma_j\sigma_j^\dagger$. The terms proportional to J^3 are neglected for an initial coherent state of the microwave (see later discussion) with its amplitude α satisfying $\alpha \ll \delta/(2J)$.

We notice that the initial state of the N_0 atoms is always in the lower spin-split levels, so that the last summation in Eq. (10) is essentially 0. For the microwave initially in a coherent state $|\alpha\rangle$ and the number of the inner-site electrons to be N_0 (in a number state $|N_0\rangle$ created by $c_j^\dagger$'s), the state for a time evolution $T = \pi\delta/J^2$ becomes $e^{-iTH'_{in}}|\alpha\rangle|N_0\rangle = |(-1)^{N_0}\alpha\rangle|N_0\rangle$, where $|(-1)^{N_0}\alpha\rangle$ is a coherent state of the microwave with amplitude $(-1)^{N_0}\alpha$. It can be seen that this result is consistent with Eq. (8). We also notice that $U, U^\dagger$ in Eq. (10) can be realized through adiabatically tuning the gap of the inner-site electrons into resonance with the microwave and then adjusting the phase ϕ to be $\pi/2, -\pi/2$ respectively for a time evolution $t = 1/\delta$ (see Eq. (9) and Fig. 3(a)). The microwave is stored in a quantum memory [42, 43] in the process of tuning the gap of the inner-site electrons. Hence the derivation is finished. Experimentally [29], $\omega_m/(2\pi) \sim 114.31$ GHz, $\Omega/(2\pi) \sim 120.74$ GHz (0.5 meV), $J/(2\pi) \sim 214$ MHz, $\alpha \sim 1.5$ and $T \sim 70$ ns. If we choose $T = \pi\delta/(2J^2)$ instead of $\pi\delta/J^2$, the state will evolve to $|(i)^{N_0}\alpha\rangle|N_0\rangle$ which can still be used to measure the parity of N_0. However, despite the advantage of shorter time, measuring the corresponding four coherent states will involve higher error rates (> 0.01) [44].

IV. USEFUL ENTANGLEMENT RESOURCE

The conditionally entangled states in Eq. (7) are not a useful entanglement resource: e.g. one cannot test Bell inequalities [45] or perform quantum computing [27] for these states. This is because the two levels of one subsystem of the entangled states are represented by the absence ($|0\rangle$) and presence ($|1\rangle$) of a fermion in a single

site. Due to the superselection rule [22], it is rather difficult to prepare an arbitrary superposition states between the two levels with different fermionic parity: $\alpha|0\rangle+\beta|1\rangle$, $(|\alpha|^2+|\beta|^2=1)$. We notice that there are proposals utilizing MFs to create entangled qubits [33, 46]. For one or both of the qubits, the basis is encoded with states of different fermionic parity. Thus, the experimental manipulation might be challenging, unless the spin degrees of freedom of the quantum dots are used as qubit basis [47]. A natural question arises: can we prepare useful entangled qubits from the states in Eq. (7)? The answer is yes if we encode the qubit in a logical basis by using two fermionic sites [23], e.g. $|\bar{0}\rangle \equiv |10\rangle, |\bar{1}\rangle \equiv |01\rangle$. In another word, a well-defined qubit is a parafermion that can be constructed from fermionic particle-partilce (or partilce-hole) pairs [21]. If we can achieve the encoding, then the general single-qubit unitary operations can be realized. This is because the Hadamard gate can be realized by the hopping between the two fermionic sites, and the $\pi/8$ gate can also be realized through applying biased electric field on the two sites; combining these gates together can fulfil any local unitary gates [48].

Now, the question becomes how to realize the logical-basis encoding. This can be done through the following scheme. Suppose all the sub-chains are initialized in the even-parity ground states $|G_1\rangle$ in Eq. (7). Then we measure the parity of the inner-site electrons of the chain C_1 and C_3 by using the scheme in Sec. III. Assume the results are both odd. So, the initial state of the sites $1,2,3,4$ is

$$|\psi\rangle_{1234} = \frac{|10\rangle+|01\rangle}{\sqrt{2}}\frac{|10\rangle+|01\rangle}{\sqrt{2}} \tag{11}$$

Then, we swap the states of the sites 2 and 3 through the time evolution with the Hamiltonian $H_{23} = -w(c_2^\dagger c_3 + c_3^\dagger c_2)$. Note that $\exp(-itH_{23}) = |00\rangle\langle 00| + |11\rangle\langle 11| - i|01\rangle\langle 10| - i|10\rangle\langle 01|$ when $t=\frac{\pi}{2w}$. So we have

$$e^{-itH_{23}}|\psi\rangle_{1234} = \frac{1}{\sqrt{2}}[|10\rangle_{13}(\frac{-i|10\rangle_{24}+|01\rangle_{24}}{\sqrt{2}}) + |01\rangle_{13}(\frac{|10\rangle_{24}-i|01\rangle_{24}}{\sqrt{2}})], \tag{12}$$

where we have grouped the states of the site 1 and 3 together (and also for $2,4$). Here a phase factor $-i$ is present in the result of the swap operation, indicating a nonideal interchange of the two sites' states. It can be seen that we have obtained a maximally entangled state with two qubits encoded by four fermionic sites: the sites $1,3$ for one qubit and $2,4$ for the other. The logical basis are $|\bar{0}\rangle_1 \equiv |10\rangle_{13}$, $|\bar{1}\rangle_1 \equiv |01\rangle_{13}$ for the first qubit, and $|\bar{0}\rangle_2 \equiv |10\rangle_{24}$, $|\bar{1}\rangle_2 \equiv |01\rangle_{24}$ for the second. In fact, the success of creating this entangled state is attributed to the phase factor $-i$ mentioned earlier; without it the above process is not possible [49]. See Fig. 5 for the schematic diagram of the swap operation.

The state (12) is useful as discussed in the first paragraph of the present section. But one drawback is that

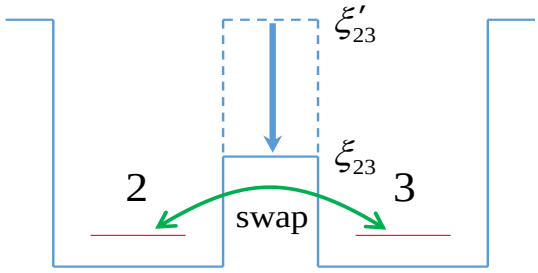

FIG. 5. (color online). The schematic diagram of the swap operation. ξ'_{23} is the potential barrier between the quantum dot 2 and 3 (see Fig. 2(c)). The barrier is sufficiently high so that the coupling between the two quantum dots is switched off. When the barrier is suddenly decreased from ξ'_{23} to a lower value ξ_{23}, the hopping interaction between the two sites is induced (see the green line with arrows). This interaction results in the swap operation as shown in Eq. (12). The decrease of the barrier is realized through increasing the gate voltage between the two sites. See Fig. 3(b). After the swap operation is finished, the barrier is restored to the higher value ξ'_{23} in order to switch off the interaction between the two sites.

the site 3 is far from the site 1 so that it is difficult to induce interaction between them (similar for the site 2 and 4). This problem can be solved by using the chain $C_{1'}$ and $C_{3'}$ as shown in Fig. 2 (a). These chains are both in the conditionally maximally entangled states as C_1 and C_3. Then, one can perform teleportation to transfer the state of the site 3 to $1'$ and that of 2 to $4'$. The detailed scheme is discussed in the Appendix C. Finally, we obtain a useful maximally entangled state with two logical qubits encoded by the sites $1,1'$ and $4,4'$ respectively. See Fig. 2(d).

The above scheme is still feasible when the measurement result for the parity of the inner-site electrons of C_1 and/or C_3 is even. But the final entangled state is a little different. For instance, if the parity of the inner sites of C_1 is even, the logical basis for the qubit in the sites $1,1'$ will be $|\bar{0}\rangle_1 \equiv |00\rangle_{11'}$, $|\bar{1}\rangle_1 \equiv |11\rangle_{11'}$. In fact, the local gates for correcting the bit-flip errors or phase errors in the teleportation in Eq. (C3) is dispensable for achieving the final entangled qubits. For instance, if the bit-flip gates are not performed, the basis of the relevant qubit will change from $\{|00\rangle, |11\rangle\}$ to $\{|10\rangle, |01\rangle\}$ (or reversely), but the entanglement is equivalent. The situation that any of the chains are in the state $|G_2\rangle$ in Eq. (7) is similar. So we omit the discussion.

Finally, we would like to remark that all the measurements for determining the parity can be postponed after the operation of swap (Fig. 2(c)) and/or Bell measurement (Fig. 2(d)) is performed. This is valid because of the linearity of quantum evolution.

V. CONCLUSION

We have shown that a pair of maximally entangled solid-state charge qubits can be extracted from two parallel chains of coupled quantum dots that support zero-energy edge modes. The edge mode is composed of unpaired Majorana fermions. The extracted entanglement is a useful resource for quantum computing [27]. The details of the entangled state depends on both the parity measurement of the inner-site electrons in each chain (see Eq. (7)) and the teleportation between the chains. Our scheme provides an illustration of *localizable entanglement* [19, 20], which is feasible under realistic experimental conditions, as it allows for finite temperature effect and local noise. That is, the ground state of the chain is protected against thermal excitations due to the substantial energy gap, and it is also topologically protected against local perturbation on the bulk because the zero-energy mode is localized at the edges [18]. Moreover, it is only required to finely tune the system parameters close to the boundary sites (See Eq. (4)), while small disorders in the inner sites (the bulk of the chain) is allowed. The total operation time of our scheme is around 300 ns which is within the decoherence time $\sim$ 700 ns mainly due to the Johnson-Nyquist noise of the electrical gates [23]. As fluctuations of the environmental charges trapped in the insulating substrate or at the interface of the heterostructure may further reduce the coherence time [24], new growth methods for materials with low trapped charge density [25], as well as the charge echo techniques [26], can alleviate the decoherence. The operation time can in principle be reduced through increasing the interaction strength between the microwave (frequency ω_m) and the quantum dots (resonant frequency of the spin-split levels Ω). See the last paragraph of Sec. III. The values of Ω and ω_m should also be increased correspondingly for the rotating-wave approximation in Eq. (9) to be valid. Future work can be pursued on the scenarios that the disorders close to the boundary sites are present and/or the disorders in the bulk are too large, for which the degree of the extracted entanglement will generally decrease.

ACKNOWLEDGMENTS

Li Dai would like to thank Yu-Chin Tzeng, Yi-Hao Jhu and Radhakrishnan Chandrashekar for helpful discussions, and also Ying Li for mentioning localizable entanglement during Li Dai's previous postdoctoral research in Singapore. Li Dai is supported by the Research Grant Number: 102-2811-M-005-013 in Taiwan. M.-C. Chung is supported by the MOST Grant under the Contract Number: 102-2112-M-005-001-MY3.

Appendix A: Bogoliubov-de Gennes transformation

One can use the Bogoliubov-de Gennes transformation [50] to solve for the zero mode

$$\begin{aligned}\tilde{b}_j =&\frac{1}{2}\sum_{k=1}^{N}\left[\phi_{j,k}d_{2k-1}+i\psi_{j,k}d_{2k}\right],\\ =&\frac{1}{2}\sum_{k=1}^{N}\left[(\phi_{j,k}-\psi_{j,k})c_k^\dagger+(\phi_{j,k}+\psi_{j,k})c_k\right],\\ &(j=1,2,\cdots,N),\end{aligned}\tag{A1}$$

where $\phi_{j,k}$ and $\psi_{j,k}$ are real coefficients determined by the condition that the Hamiltonian (1) is diagonalized: $H=\sum_{j=1}^{N}\lambda_j(\tilde{b}_j^\dagger\tilde{b}_j-\frac{1}{2})$. We note that $[\tilde{b}_j,H]=\lambda_j\tilde{b}_j$. If there exists a zero mode, say $\lambda_N=0$, we have $[\tilde{b}_N,H]=0$. $[\tilde{b}_N,H]$ can be calculated by using Eq. (1) and (A1). By requiring the coefficients of c_j and $c_j^\dagger$ in the calculated result to be zero, we get

$$\begin{aligned}&\begin{pmatrix}\phi_{N,j+1}\\ \phi_{N,j}\end{pmatrix}=\begin{pmatrix}\frac{-\mu_j}{\Delta_j+w_j} & \frac{\Delta_{j-1}-w_{j-1}}{\Delta_j+w_j}\\ 1 & 0\end{pmatrix}\begin{pmatrix}\phi_{N,j}\\ \phi_{N,j-1}\end{pmatrix},\\ &\begin{pmatrix}\psi_{N,j-1}\\ \psi_{N,j}\end{pmatrix}=\begin{pmatrix}\frac{-\mu_j}{\Delta_{j-1}+w_{j-1}} & \frac{\Delta_j-w_j}{\Delta_{j-1}+w_{j-1}}\\ 1 & 0\end{pmatrix}\begin{pmatrix}\psi_{N,j}\\ \psi_{N,j+1}\end{pmatrix},\\ &(j=1,2,\cdots,N),\end{aligned}\tag{A2}$$

where the variables with subscripts equal to $(N,0)$ or $(N,N+1)$ are assumed to be 0. For a uniform chain i.e. $w_j=w$, $\Delta_j=\Delta$ and $\mu_j=\mu$ in the above two equations, we notice that the transfer matrices are identical: $\begin{pmatrix}\frac{-\mu}{\Delta+w} & \frac{\Delta-w}{\Delta+w}\\ 1 & 0\end{pmatrix}\equiv A$. However, the index for $\phi_{N,i}$ will increase upon the action of the transfer matrix, while for $\psi_{N,i}$ the index will decrease. So, we can set $\psi_{N,j}=\phi_{N,N+1-j}$, and the Bogoliubov-de Gennes transformation (A1) for d_N becomes

$$\begin{aligned}\tilde{b}_N=&\frac{1}{2}\sum_{k=1}^{N}\left[\phi_{N,k}(d_{2k-1}+id_{2(N+1-k)})\right],\\ =&\frac{1}{2}\sum_{k=1}^{N}\left[\phi_{N,k}(c_k+c_k^\dagger+c_{N+1-k}-c_{N+1-k}^\dagger)\right]\end{aligned}\tag{A3}$$

Suppose the two eigenvalues of the transfer matrix A are λ_1 and λ_2, i.e. $A|\lambda_i\rangle=\lambda_i|\lambda_i\rangle$, $i=1,2$, so $A^{-1}A|\lambda_i\rangle=|\lambda_i\rangle=\lambda_iA^{-1}|\lambda_i\rangle$, thus the two eigenvalues of A^{-1} are λ_1^{-1} and λ_2^{-1} (for $\lambda_i\neq0$). If $|\lambda_1|<1$ and $|\lambda_2|<1$ (or, $|\lambda_1^{-1}|<1$ and $|\lambda_2^{-1}|<1$), we will have a decaying solution for $\phi_{N,i}$ (or $\phi_{N,N+1-i}$), $i=1,2,\cdots,N$, in the thermodynamic limit $N\to\infty$. This corresponds to $|\mu|<2w$. For general values of w_j, Δ_j and μ_j, Ref. [29] proves that if w_j and Δ_j are sign-ordered i.e. sign(Δ_jw_j)=sign($\Delta_{j+1}w_{j+1}$), and $|\mu_j|<\max(|w_{j-1}|,|\Delta_{j-1}|)$, then the chain has zero-mode Majoarana fermions. The solution (4) can be verified by substituting it into Eq. (A2). Actually, there is another

solution: $\mu_1 = \mu_N = 0$, $\Delta_1 = -w_1$, $\Delta_{N-1} = -w_{N-1}$, corresponding to the absence of d_2 and d_{2N-2} in Eq. (3). The two MFs form a zero-energy edge mode that is similar to Eq. (5). Further analysis for this solution is also very similar to that for Eq. (4) and omitted.

Next, we prove the parity equality: $\prod_{j=1}^{N}(1-2c_j^\dagger c_j) = \prod_{j=1}^{N}(1-2\tilde{b}_j^\dagger \tilde{b}_j)$. The Hamiltonian (3) can be written as $H = \frac{i}{4}\sum_{l,m} A_{l,m} d_l d_m$. The coefficient matrix A is block diagonalized by a $2N \times 2N$ real orthogonal matrix W: $A_{j,k} = \sum_{m,n} W_{j,m}^T \Lambda_{m,n} W_{n,k}$, where Λ is a block diagonal matrix: $\Lambda_{2k-1,2k} = -\Lambda_{2k,2k-1} = \lambda_j$ (other matrix elements are zero). Note that $WW^T = W^T W = I$ so that $(\det W)^2 = \det W \det W^T = \det(WW^T) = 1$. When $\det W = 1$, the parity equality holds [31]. For the parameters value in Eq. (4), we have the zero-energy mode in Eq. (5). The corresponding W will be $W_{j,1} = \delta_{j,2N-1}$, $W_{j,2N} = W_{2N,j} = \eta\delta_{j,2N}$, $W_{2N-1,j} = \delta_{j,1}$ for $1 \le j \le 2N$. While $W_{j,k} = (W_0)_{j,k-1}$ for $1 \le j \le 2N-2$, $2 \le k \le 2N-1$. Here $\eta = \det W_0$ is defined in Eq. (5). Therefore, $\det W$ can be calculated, according to the definition of determinant, as $\det W = \eta \det W_0 = \eta^2 = 1$. This concludes the proof.

Appendix B: Ground states in real space of the chain

In real space of the chain, $|G_1\rangle$ can be written as

$$|G_1\rangle = \sum_{i,j=0}^{1} z_{ij} |ij\rangle_{1,N} |\Psi_{ij}\rangle, \tag{B1}$$

where we have grouped the states for the sites 1 and N together (assume $N \ge 3$ first), and $|\Psi_{ij}\rangle$ is the state for the sites from 2 to $N-1$. We notice that because $|G_1\rangle$ has an even parity (i.e. it is a superposition of the states with an even number of electrons), the states $|\Psi_{00}\rangle$ and $|\Psi_{11}\rangle$ also have an even parity, while the states $|\Psi_{01}\rangle$ and $|\Psi_{10}\rangle$ have an odd parity.

The state $|G_1\rangle$ satisfies $\tilde{b}_N|G_1\rangle = 0$. By using Eq. (5), we have $\tilde{b}_N|G_1\rangle$ equal to

$$|00\rangle_{1,N}(z_{10}|\Psi_{10}\rangle - \eta z_{01}|\Psi_{01}\rangle) + |01\rangle_{1,N}(z_{11}|\Psi_{11}\rangle - \eta z_{00}|\Psi_{00}\rangle) + |10\rangle_{1,N}(z_{00}|\Psi_{00}\rangle - \eta z_{11}|\Psi_{11}\rangle) + |11\rangle_{1,N}(z_{01}|\Psi_{01}\rangle - \eta z_{10}|\Psi_{10}\rangle).$$

We can set $z_{10} = \eta z_{01} \equiv x_1/\sqrt{2}$, $z_{00} = \eta z_{11} \equiv x_0/\sqrt{2}$, $|\Psi_{10}\rangle = |\Psi_{01}\rangle \equiv |S_e\rangle$, $|\Psi_{00}\rangle = |\Psi_{11}\rangle \equiv |S_o\rangle$ (note that $\eta^2 = 1$). Therefore, $|G_1\rangle$ equals

$$x_0 \frac{|00\rangle_{1,N} + \eta|11\rangle_{1,N}}{\sqrt{2}} |S_e\rangle + x_1 \frac{|10\rangle_{1,N} + \eta|01\rangle_{1,N}}{\sqrt{2}} |S_o\rangle, \tag{B2}$$

We note that $\langle G_1|c_N^\dagger c_1^\dagger c_1 c_N|G_1\rangle = \frac{1}{2}|x_0|^2$. For the homogeneous chain ($\Delta_j = \Delta$, $w_j = w$, $\mu_j = \mu$), if we further have $\Delta = w > 0, \mu = 0$, the Hamiltonian (3) reduces to $H = iw\sum_{j=1}^{2N-1} d_{2j} d_{2j+1}$ and the new Dirac fermion operators that diagonalize the Hamiltonian (3) are $\tilde{b}_j = (c_{2j} + ic_{2j+1})/2$, $\tilde{b}_j^\dagger = (c_{2j} - ic_{2j+1})/2$, for $j = 1, 2, \cdots, N-1$, ($\eta = 1$, see Ref. [31] for details). These relations together with Eq. (2) and (5) can be used to solve for c_1 and c_N.

$$\begin{aligned} c_1 &= \frac{1}{2}(\tilde{b}_N + \tilde{b}_N^\dagger + i\tilde{b}_1 + i\tilde{b}_1^\dagger), \\ c_N &= \frac{1}{2}(\tilde{b}_N - \tilde{b}_N^\dagger - i\tilde{b}_{N-1} + i\tilde{b}_{N-1}^\dagger). \end{aligned} \tag{B3}$$

So $\langle G_1|c_N^\dagger c_1^\dagger c_1 c_N|G_1\rangle$ can be calculated by using the above expressions and Eq. (6), and the result is $\frac{1}{4}$. Thus, x_0 can be chosen as $\frac{\sqrt{2}}{2}$, and x_1 is determined by normalization condition of the state (7): $|x_0|^2 + |x_1|^2 = 1$, so $x_1 = \frac{\sqrt{2}}{2}$. For general values of Δ_j, w_j, μ_j, we only have Eq. (2) and (5), but $\tilde{b}_j$ ($j = 1, 2, \cdots, N-1$) is unknown, which is a function of $c_k, c_k^\dagger$ ($k = 1, 2, \cdots, N$) and can be obtained by diagonalizing the coefficient matrix in the Hamiltonian (1). Then, we can solve for c_1 and c_N to determine x_0, x_1, η in the state (7). The state $|G_2\rangle = \tilde{b}_N^\dagger|G_1\rangle$ by using Hermitian conjugate of Eq. (5). For the situation $N = 2$, the calculation is similar, where the two ground states are those before $|S_e\rangle$ and $|S_o\rangle$ in Eq. (B2).

Appendix C: Teleportation

The conditionally entangled states in Eq. (7) are useful for performing quantum teleportation. Suppose the boundary sites are in the state: $\frac{1}{\sqrt{2}}(|00\rangle_{1,N} + |11\rangle_{1,N})$. We have an extra fermion site with the index 0. The quantum state of this site may be correlated with its environment. Denote the state of the site 0 and its environment as $|\chi_0\rangle = y_0|0\rangle_0|\phi_0\rangle + y_1|1\rangle_0|\phi_1\rangle$, where $|0\rangle_0$ ($|1\rangle_0$) means that there is no (one) fermion in the site 0, y_0 and y_1 are the amplitudes, and $|\phi_0\rangle$ and $|\phi_1\rangle$ are some states of the environment. The task is to teleport the state in the site 0 to the site N. As we know, one need to perform Bell measurement. This seems not possible, but we can realize it indirectly through basis transformation in the Hilbert space of the site 0 and 1.

The initial state is

$$|\phi\rangle = |\chi_0\rangle \frac{|00\rangle_{1,N} + |11\rangle_{1,N}}{\sqrt{2}} \tag{C1}$$

Then the interaction (hopping and pairing) between the sites 0 and 1 is switched on, and their chemical potential is finely tuned to be zero. The Hamiltonian is

$$H_{01} = -w_0(c_0^\dagger c_1 + c_1^\dagger c_0) + \Delta_0(c_0 c_1 + c_1^\dagger c_0^\dagger) \tag{C2}$$

Choose the hopping amplitude w_0 and the superconducting gap Δ_0 to satisfy $w_0 = \Delta_0 > 0$. The time evolution operator is $\exp(-itH_{01})$. Setting $t = t_0 \equiv \frac{\pi}{4\Delta_0}$, we have

$$\begin{aligned} e^{-it_0 H_{01}}|\phi\rangle = \frac{1}{2}[&|00\rangle_{01}(y_0|0\rangle_N|\phi_0\rangle - iy_1|1\rangle_N|\phi_1\rangle) \\ &+|01\rangle_{01}(y_0|1\rangle_N|\phi_0\rangle - iy_1|0\rangle_N|\phi_1\rangle) \\ &+|10\rangle_{01}(-iy_0|1\rangle_N|\phi_0\rangle + y_1|0\rangle_N|\phi_1\rangle) \\ &+|11\rangle_{01}(-iy_0|0\rangle_N|\phi_0\rangle + y_1|1\rangle_N|\phi_1\rangle)], \end{aligned} \tag{C3}$$

where we have written the states of the sites 0 and 1 first, and then the states of the site N and the environment of the site 0. It can be seen that we have four results when measuring the sites 0 and 1 in the number basis: ij, $i,j \in \{0,1\}$ (see Ref. [23] for the experimental realization of charge measurement). For each result, the corresponding state for the site N and the environment of the site 0 is equivalent to the original state $|\chi_0\rangle$ up to a local unitary transformation (gate) on the site N. The results 00 and 11 involve phase gates which are fulfilled by applying electric potential, while the results 01 and 10 involve bit-flip gates which are realized by coupling the site N to a chain supporting zero-energy edge mode $\tilde{b}_m^\dagger \tilde{b}_m$. The chain has a Hamiltonian similar to Eq. (1) with parameters in Eq. (4), but N there is all replaced by another length m. The inner sites of a sub-chain in Fig. 1 can be chosen to serve as this chain. The coupling between the site N and the chain is [32]: $H_f = \kappa(c_N^\dagger - c_N)(\tilde{b}_m^\dagger + \tilde{b}_m)$, where κ denotes the coupling strength. We have $\exp(-itH_f)|0\rangle_N|G_1\rangle = i|1\rangle_N|G_2\rangle$ and $\exp(-itH_f)|1\rangle_N|G_1\rangle = i|0\rangle_N|G_2\rangle$ when $t = \pi/(2\kappa)$, realizing the bit-flip gate. Here $|G_1\rangle$ and $|G_2\rangle$ are the ground states of the chain (see Eq. (6) with N replaced by m), and their positions can be interchanged to obtain the other two Eqs. of time evolution.

For the other maximally entangled state $\frac{1}{\sqrt{2}}(|10\rangle_{1,N} + |01\rangle_{1,N})$, the discussion is very similar. We only need to flip the state of the site N in Eq. (C3) to obtain the result. See also a proposal using single-photon (boson) entanglement for teleporting photon states [51], where the situation is comparable but a difference is that the local operations in the Bob's side are performed with the aid of atom-photon interactions.

[1] Ettore Majorana, Luciano Maiani, *Ettore Majorana Scientific Papers*, 201-203 (Springer Berlin Heidelberg, 2006).
[2] F. Wilczek, Nat. Phys. **5**, 614 (2009).
[3] G. Moore and N. Read, Nucl. Phys. B **360**, 362 (1991).
[4] L. Fu and C. L. Kane, Phys. Rev. Lett. **100**, 096407 (2008).
[5] Jay D. Sau, Roman M. Lutchyn, Sumanta Tewari, and S. Das Sarma, Phys. Rev. Lett. **104**, 040502 (2010).
[6] Jason Alicea, Phys. Rev. B **81**, 125318 (2010).
[7] R. M. Lutchyn, J. D. Sau, and S. Das Sarma, Phys. Rev. Lett. **105**, 077001 (2010).
[8] L. Jiang *et al.*, Phys. Rev. Lett. **106**, 220402 (2011).
[9] M. Leijnse and K. Flensberg, Semicond. Sci. Technol. **27**, 124003 (2012).
[10] C.W.J. Beenakker, Annu. Rev. Con. Mat. Phys. **4**, 113 (2013).
[11] A. Das *et al.*, Nat. Phys. **8**, 887 (2012).
[12] M. T. Deng *et al.*, Nano Lett. **12**, 6414 (2012).
[13] H. O. H. Churchill *et al.*, Phys. Rev. B **87**, 241401(R) (2013).
[14] C. Nayak *et al.*, Rev. Mod. Phys. **80**, 1083 (2008).
[15] N.Y. Yao *et al.*, Nat. Commun. **4**, 1585 (2013).
[16] F. Konschelle and F. Hassler, Phys. Rev. B **88**, 075431 (2013).
[17] D.-L. Deng and L.-M. Duan, Phys. Rev. A **88**, 012323 (2013).
[18] P. Bonderson and C. Nayak, Phys. Rev. B **87**, 195451 (2013).
[19] F. Verstraete, M. Popp, and J. I. Cirac, Phys. Rev. Lett. **92**, 027901, (2004).
[20] M. Popp, F. Verstraete, M. A. Martín-Delgado, and J. I. Cirac, Phys. Rev. A **71**, 042306, (2005).
[21] L.-A. Wu and D. A. Lidara, J. Math. Phys, **43**, 4506 (2002).
[22] M. Skotiniotis *et al.*, Phys. Rev. Lett. **111**, 020504 (2013).
[23] L. C. L. Hollenberg *et al.*, Phys. Rev. B **69**, 113301 (2004).
[24] D. C. B. Valente, E. R. Mucciolo, and F. K. Wilhelm, Phys. Rev. B **82**, 125302 (2010).
[25] A. Zado, J. Gerlach, and D. J. As, Semicond. Sci. Technol. **27**, 035020 (2012).
[26] Y. Dovzhenko *et al.*, Phys. Rev. B **84**, 161302(R) (2011).
[27] F. Verstraete and J. I. Cirac, Phys. Rev. A **70**, 060302(R), (2004).
[28] H.-J. Briegel and R. Raussendorf, Phys. Rev. Lett. **86**, 5188, (2001).
[29] J. D. Sau and S. Das Sarma, Nat. Commun. **3**, 964 (2012).
[30] M. Leijnse and K. Flensberg, Phys. Rev. B **86**, 134528 (2012).
[31] A. Kitaev, Phys. Usp. **44**, 131 (2001).
[32] H.-F. Lü, H.-Z. Lu, and S.-Q. Shen, Phys. Rev. B **86**, 075318 (2012).

[33] P. Bonderson and R. M. Lutchyn, Phys. Rev. Lett. **106**, 130505 (2011).
[34] K. Tsujino *et al.*, Phys. Rev. Lett. **106**, 250503 (2011).
[35] H. K. Kim *et al.*, Jpn. J. Appl. Phys. **43**, 2054 (2004).
[36] D.F. Walls and Gerard J. Milburn, *Quantum Optics*, Chap. 10 (Springer, 2008).
[37] P. Yaghmaee *et al.*, Int. J. Antennas Propag. **2013**, 9 (2013).
[38] R. B. Li, L. Deng, and E.W. Hagley, Phys. Rev. Lett. **110**, 113902 (2013).
[39] M. Tavis and F. W. Cummings, Phys. Rev. **170**, 379 (1968).
[40] A. Blais *et al.*, Phys. Rev. A **69**, 062320 (2004).
[41] Simon E. Nigg and S. M. Girvin, Phys. Rev. Lett **110**, 243604 (2013).
[42] M. Afzelius *et al.*, New J. Phys. **15**, 065008 (2013).
[43] B. Julsgaard, C. Grezes, P. Bertet, and K. Mølmer, Phys. Rev. Lett. **110**, 250503 (2013).
[44] S. Izumi, M. Takeoka, K. Ema, and M. Sasaki, Phys. Rev. A **87**, 042328 (2013).
[45] J. Clauser, F. M. Horne, A. A. Shimony, and R. A. Holt, Phys. Rev. Lett. **23**, 880 (1969).
[46] Z. Wang, X.-Y. Hu, Q.-F. Liang, and X. Hu, Phys. Rev. B **87**, 214513 (2013).
[47] M. Leijnse and K. Flensberg, Phys. Rev. Lett. **107**, 210502 (2011).
[48] M. A. Nielsen and I. C. Chuang, *Quantum Computation and Quantum Information*, Sec. 4.5.3 (Cambridge University Press, Cambridge, U.K., 2000).
[49] S. R. Clark, C. M. Alves, and D. Jaksch, New J. Phys. **7**, 124 (2005).
[50] L.-J. Lang and S. Chen, Phys. Rev. B **86**, 205135 (2012).
[51] G. Björk, A. Laghaout, and U. L. Andersen, Phys. Rev. A **85**, 022316 (2012).